RESEARCH PAPER

# Silica-coated bismuth ferrite nanoparticles as novel radiosensitizers for cancer radiotherapy

***Nasim Kavousi[1], Mohammad Taghi Bahreyni Toossi[1,2]*, Hosein Azimian[1,2], Mona Alibolandi[3,4]****

*[1] Department of Medical Physics, Faculty of Medicine, Mashhad University of Medical Sciences, Mashhad, Iran*
*[2] Medical Physics Research Center, Basic Sciences Research Institute, Mashhad University of Medical Sciences, Mashhad, Iran*
*[3] Department of Pharmaceutical Biotechnology, School of Pharmacy, Mashhad University of Medical Sciences, Mashhad, Iran*
*[4] Pharmaceutical Research Center, Pharmaceutical Technology Institute, Mashhad University of Medical Sciences, Mashhad, Iran*

**ABSTRACT**

***Objective(s):*** Radiotherapy is a cornerstone of cancer treatment; however, tumor radioresistance remains a major limitation. The use of radiosensitizers offers a strategy to selectively enhance the sensitivity of malignant cells to ionizing radiation while minimizing toxicity to surrounding normal tissues. In this study, we investigated the radiosensitizing potential of silica-coated bismuth ferrite nanoparticles (BFO-Si NPs).

***Material and Methods:*** Bismuth ferrite nanoparticles (BFO NPs) were synthesized via the sol-gel method and coated with silica to produce BFO-Si NPs, and their morphology and structural properties were characterized using FESEM, EDS, HR-TEM, XRD, and DLS. Their cytotoxicity against human non-small cell lung carcinoma (NSCLC) SK-MES-1 cells was evaluated using the MTT assay. To further assess their efficacy as radiosensitizers, cell viability, colony-forming capacity, and apoptotic responses following X-ray irradiation were evaluated.

***Results:*** The BFO-Si NPs exhibited uniform spherical geometry, a narrow size distribution, and good colloidal stability. They significantly increased apoptosis induction and decreased clonogenic survival of SK-MES-1 cells under 6 MV X-ray irradiation compared with radiation alone.

***Conclusion:*** These findings demonstrate the potential of silica-coated bismuth ferrite nanoparticles as safe and effective radiosensitizers, capable of enhancing radiotherapeutic outcomes in NSCLC.

***Keywords:*** *Bismuth compounds, Radiosensitizer, lung adenocarcinoma, Radiotherapy*

**How to cite this article**

*Kavousi N, Bahreyni Toossi MT, Azimian H, Alibolandi M. Silica-coated bismuth ferrite nanoparticles as novel radiosensitizers for cancer radiotherapy. Nanomed J. 2026; 13: 1-. DOI: 10.22038/NMJ.2025.91064.2304*



## GRAPHICAL ABSTRACT

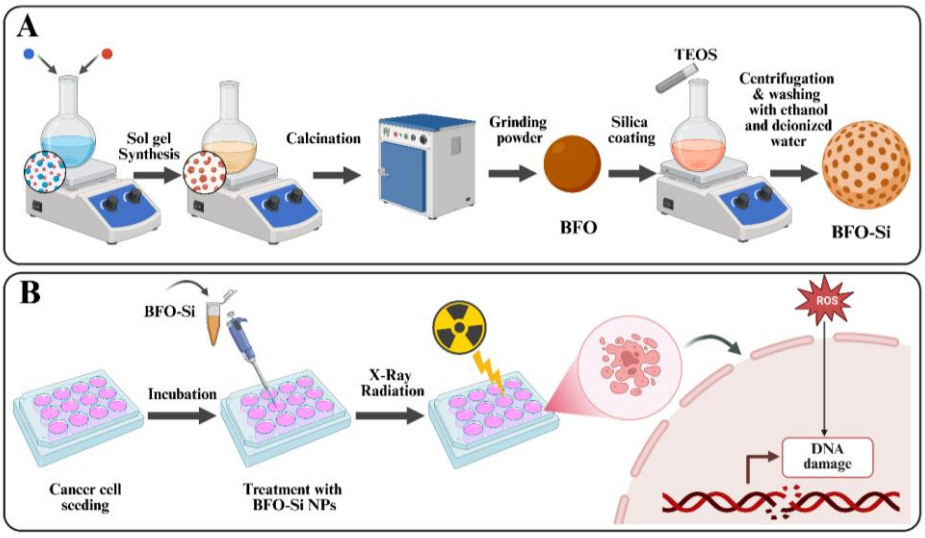


**Corresponding author(s):* Mohammad Taghi Bahreyni Toossi, Professor, Department of Medical Physics, Mashhad University of Medical Sciences, Mashhad, Iran. Email: *BahreyniMT@mums.ac.ir*;- Mona Alibolandi, Professor, Department of Medical Biotechnology, Mashhad University of Medical Sciences, Mashhad, Iran. Email: *AlibolandiM@mums.ac.ir*.

Note. This manuscript was submitted on September 08, 2025; approved on October 19, 2025.

## INTRODUCTION

Lung adenocarcinoma stands as the leading contributor to cancer-related mortality, responsible for an estimated 1.8 million fatalities reported globally in 2020 [1-3]. Patient outcomes remain poor despite significant progress in treatment modalities—including chemotherapy, targeted therapy, and radiotherapy [4]. While radiotherapy is fundamental to cancer therapy, given its capacity to manage tumor proliferation and mitigate metastatic spread, both inherent and acquired radioresistance frequently impede its therapeutic effectiveness [5]. Understanding the molecular mechanisms underlying radiosensitivity is therefore essential for improving treatment response. Addressing this limitation, nanotechnology provides a promising strategy, where nanoparticles (NPs) are being investigated as radiosensitizers to boost the therapeutic index of radiotherapy [6, 7]. Their small size, tunable surface chemistry, and multifunctionality have enabled applications in both diagnostics and therapeutics [8, 9]. In oncology, NPs have improved imaging precision and modulated tumor radiosensitivity, thereby enhancing radiation efficacy [10, 11]. High atomic number (Z) nanomaterials are particularly attractive, as they exhibit strong photoelectric absorption and energy deposition compared to soft tissue, resulting in improved radiotherapeutic effects [6]. Bismuth-based NPs, owing to their substantial atomic number (Z = 82), favorable photoelectric absorption, relative biocompatibility, and economic feasibility, have gained increasing attention as radiosensitizers [12, 13].

Historically, bismuth-containing substances have found medical applications in treating various conditions, including gastrointestinal disorders, syphilis, skin diseases, and Helicobacter pylori infections. Bismuth NPs have recently been investigated as effective CT contrast agents, radiation enhancers, and antibacterial agents [13]. As a notable multiferroic material, bismuth ferrite (BFO) exhibits both ferroelectric and magnetic behavior at ambient temperature [14]. The high atomic numbers of bismuth (82) and iron (56), combined with its magnetic characteristics, make BFO a promising candidate for multimodal imaging and image-guided Radiotherapy (IGRT). For instance, BFO NPs may serve as contrast agents for CT and magnetic resonance imaging (MRI), concurrently acting as radiosensitizers to augment local radiation dose delivery. Moreover, BFO NPs can be synthesized by scalable, cost-effective methods such as sol–gel processing [15].

However, a key challenge with magnetic NPs is their tendency to aggregate due to van der Waals forces and magnetic interactions, which reduces stability and bioavailability [16]. Surface modification is therefore essential for biomedical translation. Among various strategies, silica coating has emerged as particularly advantageous, as it improves dispersibility, prevents agglomeration, and confers hydrophilicity and biocompatibility. Silica shells also offer chemical inertness, thermal resistance, and structural stability, making them widely employed in nanomedicine [17, 18]. Furthermore, silica-based NPs can act as radiosensitizers by augmenting mitochondrial reactive oxygen species (ROS) production [19-21]. Accordingly, applying a silica shell to BFO NPs is expected to enhance their physicochemical and radiobiological performance.

Beyond these properties, silica nanomaterials are especially valuable in drug delivery [21]. Mesoporous silica nanoparticles (MSNs), characterized by tunable pore size, extensive surface area, and facile modification, exhibit high drug-loading capacity, controlled release, and integration of multifunctional therapeutic strategies. Their biodegradability, clearance, and translational potential have also established silica-based systems as promising platforms for cancer theranostics [18, 22]. Although bismuth-based nanomaterials such as $Bi_2Se_3$, $Bi_2S_3$, and uncoated BFO NPs have been evaluated as radiosensitizers [7, 23-25], these studies primarily focused on dose enhancement without incorporating drug-delivery functionality. In contrast, our silica-coated BFO (BFO-Si) system integrates a high-Z, magnetically responsive core with a mesoporous silica shell that prevents aggregation, enhances dispersibility, enables drug encapsulation with controlled release, and allows further functionalization for imaging applications. This study represents the first systematic evaluation of silica-coated BFO NPs as a dual radiosensitizing and drug-delivery/theranostic platform for non-small cell lung cancer under clinically relevant 6-MV photon irradiation. Thus, a BFO core encapsulated by a silica shell offers a multifunctional system that combines magnetic and radiosensitizing properties with chemical stability, drug-delivery capability, and potential for multimodal imaging [26]. However, their radiosensitizing efficacy in non-small cell lung cancer (NSCLC) has not been evaluated. Therefore, this study evaluates the radiosensitizing potential of BFO-Si NPs under 6-MV photon irradiation in SK-MES-1 lung carcinoma cells, particularly emphasizing their ability to enhance radiotherapy efficacy and induce apoptosis (Scheme 1).

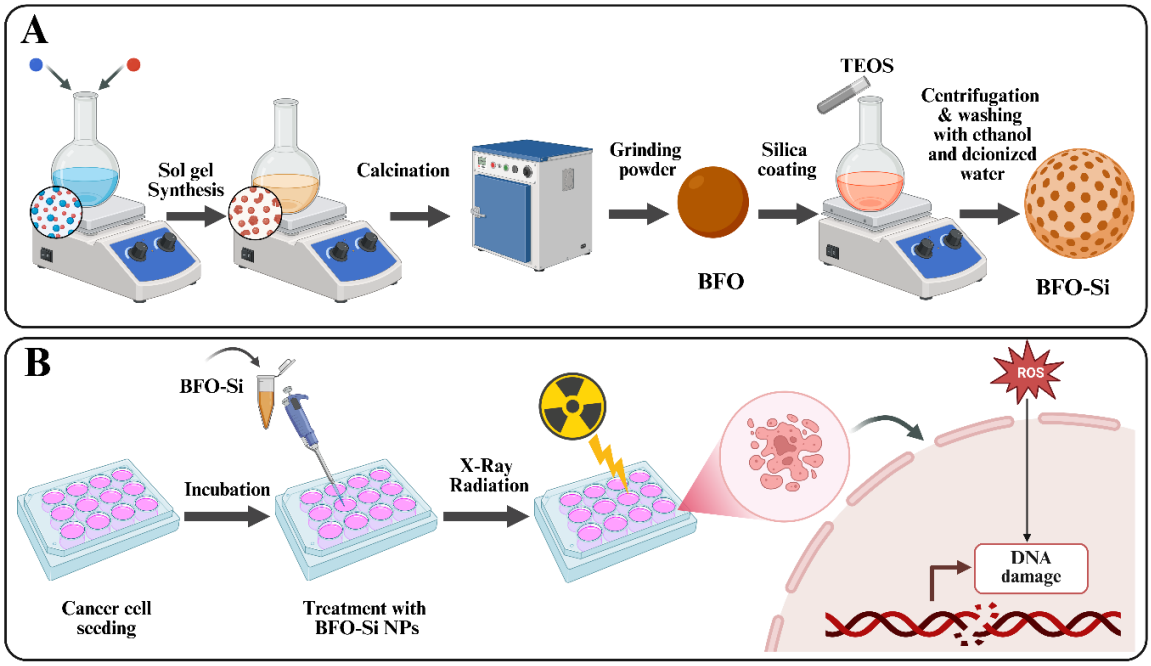


Scheme 1. Schematic overview of the study design.

## MATERIALS AND METHODS

### *Materials*

Reagents utilized included bismuth (III) nitrate pentahydrate [$Bi(NO_3)_3{\cdot}5H_2O$], iron (III) nitrate nonahydrate [$Fe(NO_3)_3{\cdot}9H_2O$], acetic acid ($CH_3COOH$), ethylene glycol (EG), Tween-80, ethanol, ammonium hydroxide, cyclohexane, tetraethyl orthosilicate (TEOS), and 3-(4,5-Dimethylthiazol-2-yl)-2,5-diphenyltetrazolium bromide (MTT), all from Sigma-Aldrich. Biological reagents, including high-glucose Dulbecco's modified Eagle's medium (H-DMEM), fetal bovine serum (FBS), phosphate-buffered saline (PBS), penicillin-streptomycin (PS), and trypsin, were supplied by Gibco. The human NSCLC cell line, SK-MES-1, was sourced from the Pasteur Institute of Iran.

### *Synthesis of BFO NPs*

Bismuth ferrite NPs ($BiFeO_3$, BFO) were synthesized via a sol-gel method. Briefly, $Bi(NO_3)_3{\cdot}5H_2O$ and $Fe(NO_3)_3{\cdot}9H_2O$ (purity >99%, Sigma-Aldrich) were dissolved in deionized water at stoichiometric ratios to obtain a uniform precursor solution. Following this, citric acid (2.5 g) was subsequently incorporated as a chelating agent. The solution was maintained under continuous agitation and heated until complete evaporation produced a gel residue. During gelation, ethylene glycol was added to promote polymerization. The detailed procedure has been described elsewhere [27]. The resulting gel was dried at 100–120 °C for 24 h to yield a xerogel. This xerogel subsequently underwent calcination at 450 °C for 2–2.5 hours in a laboratory furnace (3 °C/min heating rate). The calcined product was finely ground to obtain nanostructured BFO powders.

### *Silica Coating of Bismuth Ferrite NPs*

BFO-Si NPs were synthesized using an established protocol with some corrections [28]. Briefly, 10 mL of cyclohexane containing BFO NPs (1 mg/mL) was sonicated for 10 min, subsequently combined with 8 mL of ethanol containing Tween-80 (100 mg). The mixture underwent an additional 10 min of sonication and was stirred under argon gas for 6 hours. Subsequently, ammonium hydroxide (200 µL, 30%) and TEOS (100 µL in 2 mL of ethanol) were added sequentially, and the reaction was maintained under continuous agitation for 24 hours. The obtained BFO-Si NPs were harvested via centrifugation (12,000 rpm, 10 min) and thoroughly rinsed with ethanol and deionized water.

### *Characterization of nanoparticles*

The synthesized NPs underwent comprehensive characterization to determine their properties.

Crystalline structure was investigated through X-ray diffraction (XRD) on an X'PertPro diffractometer (Panalytical, The Netherlands). Morphological and compositional characteristics were conducted using a field-emission scanning electron microscope (FESEM, TESCAN, UK), complemented by energy-dispersive X-ray spectroscopy (EDX) capabilities, and high-resolution transmission electron microscopy (HRTEM). Furthermore, a Malvern Zetasizer Nano ZS was employed to measure the hydrodynamic size profile and surface charge of the nanocomplexes.

***Cell Culture***

SK-MES-1 non-small cell lung carcinoma cells were cultivated in high-glucose Dulbecco's modified Eagle's medium (H-DMEM) containing 10% fetal bovine serum (FBS) and 1% penicillin–streptomycin. Optimal growth conditions were provided by a humidified incubator set at 37 °C with a 5% $CO_2$ concentration.

***In vitro cytotoxicity***

The in vitro cytotoxicity of the nanoplatform was evaluated in SK-MES-1 cells using the MTT assay. During their logarithmic growth phase, cells were seeded into 96-well plates ($5\times10^3$ cells/well) and incubated to permit **sufficient** adherence. On the subsequent day, the medium was exchanged with fresh medium containing BFO or BFO-Si NPs at concentrations ranging from 1.56 to 200 µg/mL and incubated for 6 hours. Then, the treatment medium was aspirated, and the cells were further cultured in fresh medium for 48 hours. Thereafter, 20 µL of MTT reagent (5 mg/mL) was introduced to each well, and the plates were incubated for 4 hours to allow the formation of formazan crystals by metabolically active cells. The MTT solution was discarded, and DMSO (100 µL/well) was added to dissolve the crystals. A microplate reader quantified cell viability by measuring absorbance at 570/630 nm.

***Irradiation procedure on cells***

Cell irradiation (2, 4, 6, and 8 Gy) was performed using a 6 M Elekta Compact linear accelerator (Sweden). The photon beam was delivered through a 20 × 20 $cm^2$ radiation field, with culture plates positioned on five 1-cm-thick layers of tissue-equivalent material to ensure uniform dose distribution. The procedure was conducted with the gantry fixed at 180°, employing the source-to-axis distance (SAD) technique.

***In vitro radio-enhancement of NPs***

The radiosensitizing potential of BFO and BFO-Si NPs was quantitatively determined via an MTT assay. SK-MES-1 cells were cultured in 96-well plates ($5\times10^3$ cells/well) and maintained at 37 °C in a 5% $CO_2$ atmosphere for 24 hours. Following adherence and initial growth, the cells were subjected to a 6-hour co-incubation with BFO-Si NPs (15 µg/mL). After this, X-ray radiation was applied at target doses of 2 and 4 Gy. After an additional 48 h incubation, the MTT assay determined cell viability to evaluate the radiosensitizing efficiency of the NPs.

***Clonogenic Assay for Evaluating the Radiosensitizing Effect of Synthesized NPs***

A clonogenic assay was performed to assess the radiosensitizing efficacy of the prepared NPs by measuring the capacity of SK-MES-1 cells to retain proliferative capacity and form colonies after irradiation. Cells were initially seeded in 6-well plates at varying densities of 800, 1000, 1200, 1400, and 2400 cells per well and incubated for 24 hours to permit adherence. Following PBS washing, cells were treated with BFO-Si NPs (15µg/mL) for 6 hours. The medium was then exchanged, and cells underwent X-ray irradiation. Irradiation doses were precisely matched to the initial seeding density: 2 Gy (1000 cells/well), 4 Gy (1200 cells/well), 6 Gy (1400 cells/well), and 8 Gy (2400 cells/well). The 800-cell group served as the non-irradiated control. Following irradiation, cells were incubated for 12 days to permit colony formation. Post-incubation, colonies underwent PBS washing, methanol fixation, and Giemsa staining for 30 minutes. Plates were then gently rinsed with water and air-dried at ambient temperature. Colony enumeration was restricted to those comprising over 50 cells. Plating Efficiency (PE) was derived from the ratio of formed colonies to the initial number of seeded cells. The surviving fraction (SF) at each specific radiation dose was defined as the PE of irradiated samples normalized to that of the non-irradiated control.

***Apoptosis assay***

The apoptotic response was estimated via Annexin V-FITC/propidium iodide (PI) staining, evaluating the effects of X-ray irradiation (2 Gy and 4 Gy) with and without BFO-Si NPs. SK-MES-1 cells were cultured in 12-well plates and grown for 24 hours before treatment. The medium was then exchanged for fresh DMEM containing BFO-Si NPs (15 µg/mL) for 6 hours, while control cells received only DMEM. Following nanoparticle removal and PBS washing, fresh medium was supplied. The

cultures were irradiated at 2 Gy and 4 Gy and incubated overnight. Post-treatment, cells were collected, subjected to two PBS washes, and prepared for resuspension in Annexin V binding buffer (500 µL). Staining was conducted with 5 µL each of Annexin V-FITC and PI. Flow cytometric analysis was performed, and data were analyzed using FlowJo version 7.6. Non-irradiated samples were processed in parallel as controls for comparison.

***Statistical analysis***

Values are presented as mean ± standard deviation (SD)**.** Comparisons among multiple groups and the control were conducted using one-way ANOVA via GraphPad Prism. Statistical significance is indicated as $P < 0.05$ *(*), $P < 0.01$ (**), $P < 0.001$ (***)***,*** and $P < 0.0001$ *(****)*.

**RESULTS AND DISCUSSION**

***Characterization***

***The morphology of BFO and BFO-Si NPs***

The morphology, particle dimensions, and spatial distribution of the synthesized NPs were investigated using FESEM and EDS. FESEM images of BFO and BFO-Si NPs (Fig. 1A, B) revealed predominantly spherical morphologies with mean diameters of ~40 nm (BFO) and ~65 nm (BFO-Si), both smaller than the corresponding hydrodynamic sizes obtained by dynamic light scattering (DLS) (Table 1). HRTEM confirmed these findings; a representative micrograph of BFO-Si (Fig. 1C) showed spherical particles with an average diameter of ~54 nm. These findings align with earlier studies on BFO-based nanostructures of comparable dimensions [23, 29]. The EDS spectrum of BFO (Fig. 2A) showed only Bi, Fe, and O peaks, verifying phase-pure $BiFeO_3$ construction. The Bi/Fe atomic ratio was 1.1028, closely matching the theoretical 1:1 stoichiometry. In BFO-Si NPs, EDS confirmed the presence of Bi, Fe, Si, O, and C, with no extraneous elements, indicating successful silica incorporation. Elemental mapping further demonstrated the homogeneous distribution of Bi, Fe, O, and Si within BFO-Si NPs (Fig. 2B), confirming uniform integration of silica with the bismuth ferrite matrix.

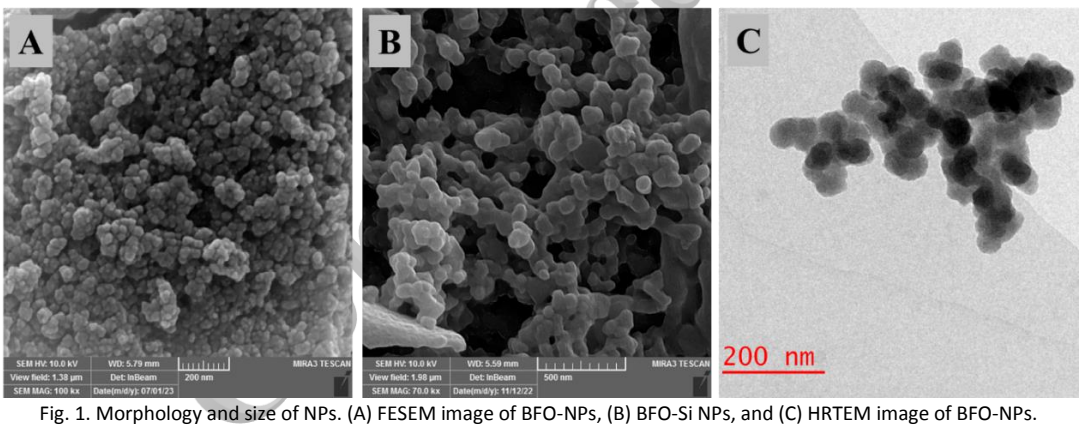


Fig. 1. Morphology and size of NPs. (A) FESEM image of BFO-NPs, (B) BFO-Si NPs, and (C) HRTEM image of BFO-NPs.

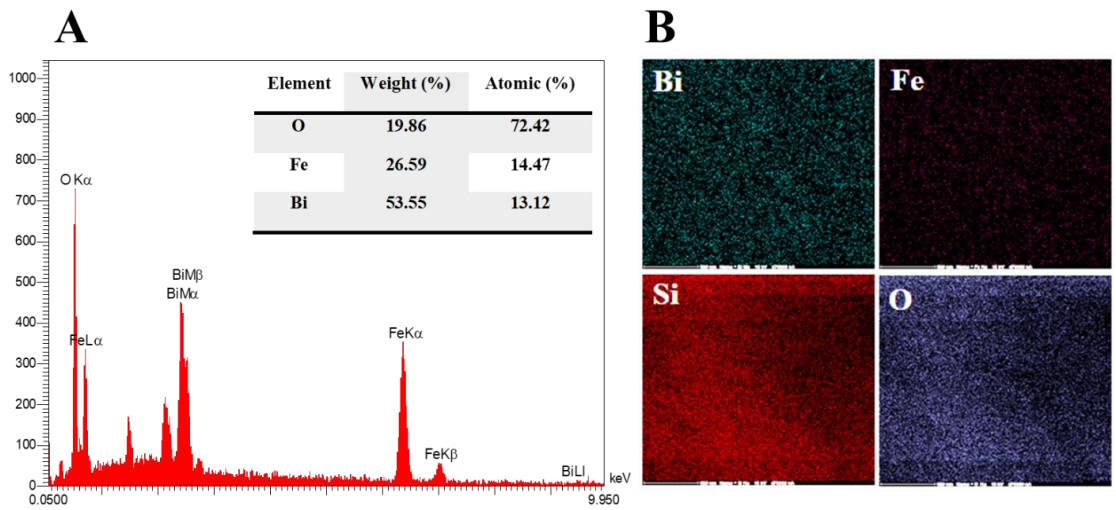


Fig. 2. (A) EDS analysis for BFO NPs. (B) FESEM-EDS elemental mapping analysis of BFO-Si NPs.

Table 1. DLS and zeta potential measurements of the prepared NPs.

| Sample | Z-average (nm) | PDI | Zeta potential (mV) |
|---|---|---|---|
| BFO | 82.73±1.24 | 0.20±0.015 | -37 |
| BFO-Si | 113.78±2.67 | 0.26±0.02 | -30 |

***XRD analysis***

The crystalline properties of the synthesized NPs were characterized using XRD. The diffraction pattern of BFO NPs (Fig. 3, A) revealed peaks that can be indexed to a rhombohedral perovskite phase, consistent with the reference data (JCPDS card), confirming the formation of the BFO phase. For BFO-Si NPs (Fig. 3, B), a broad halo observed in the 2θ range of 10–80° was attributed to the amorphous silica, while the characteristic reflections of the BFO crystalline core remained intact [30]. This indicates that silica coating did not disrupt the underlying crystal structure of the BFO NPs. The mean BFO crystallite size, derived from the (110) reflection using the Scherrer equation, was ~45 nm, in close agreement with HRTEM observations. Previous studies have similarly reported rhombohedral perovskite structures for BFO with minimal secondary phases and crystallite sizes ranging from 34–48 nm, depending on synthesis conditions [31-33]. These results confirm that silica modification preserves the intrinsic crystallinity of BFO.

***Size distribution and zeta potential***

DLS analysis revealed mean hydrodynamic diameters of 82.73 nm for BFO and 113.78 nm for BFO-Si (Table 1). These values are larger than the particle sizes determined by FESEM and HRTEM (40–65 nm), as expected due to solvation effects and the hydrodynamic layer surrounding the particles in suspension. The observed increase in size following silica coating further confirms successful surface modification. Zeta potential measurements yielded −37 mV for BFO and −30 mV for BFO-Si, indicating moderately high negative surface charges (Table 1). These values reflect good colloidal stability in aqueous suspension, which is advantageous for biomedical applications by minimizing aggregation and supporting drug delivery potential.



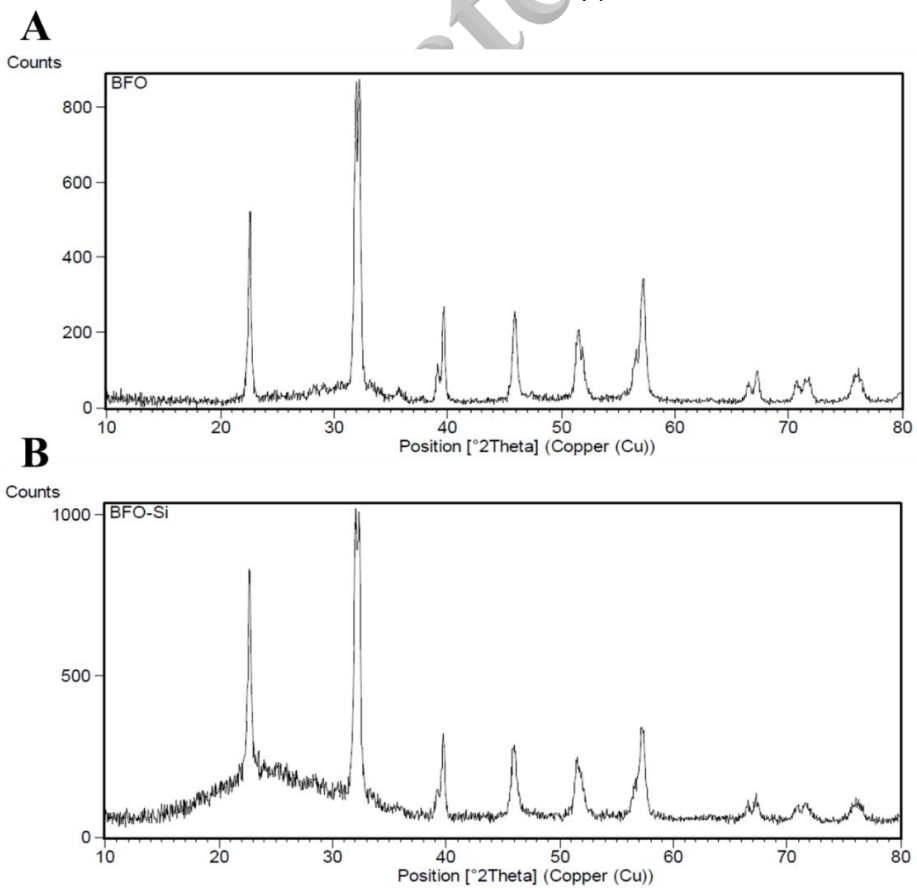


Fig. 3. (A) XRD pattern of BFO NPs, and (B) BFO-Si NPs.

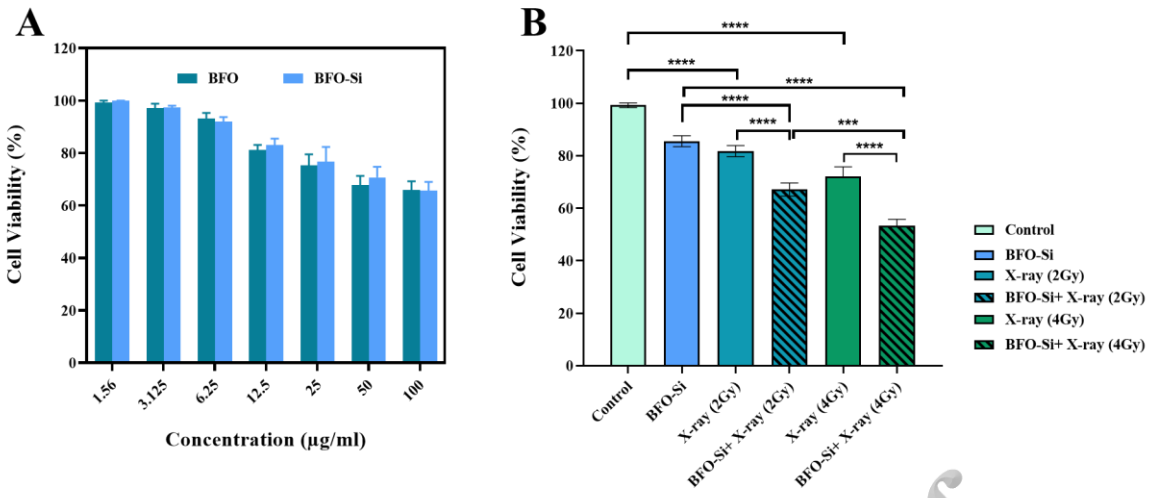


Fig. 4. (A) Viability of SK-MES-1 cells following treatment with different BFO and BFO-Si NPs concentrations. (B) cell viability of SK-MES-1 cells under 2 Gy and 4 Gy X-ray irradiation, and after treatment with the prepared BFO-Si NPs with and without X-ray irradiation. Differences were considered statistically significant at ***$p < 0.001$, ****$p < 0.0001$.

***Cytotoxicity assay***

Biocompatibility and low cytotoxicity are essential prerequisites for nanoparticle-based biomedical applications. The in vitro cytotoxicity of BFO and BFO-Si NPs was assessed using the MTT assay. Both NPs exhibited cell viability above 70% at concentrations up to 25 µg/mL (Fig. 4A), indicating favorable biocompatibility and minimal cytotoxicity. Accordingly, a 15 µg/mL BFO-Si NPs concentration was selected for subsequent experiments. These findings are consistent with previous reports demonstrating that BFO-based nanomaterials possess low cytotoxicity and high biocompatibility at similar concentration ranges [23, 34, 35].

***Effect of BFO-Si NPs under X-ray irradiation on SK-MES-1 cell viability***

The radiosensitizing effect of BFO-Si NPs was assessed in SK-MES-1 cells by MTT assay following X-ray irradiation at 2 and 4 Gy, with or without 15 µg/mL BFO-Si NPs (Fig. 4B). Statistical analysis revealed significant differences between groups, indicating that irradiation reduced cell viability and that BFO-Si NPs further amplified this effect. Irradiation with 2 Gy decreased viability to 81.8%, whereas co-treatment with BFO-Si NPs reduced it to 67.0%, demonstrating enhanced radiation sensitivity. A dose-dependent decline in viability was observed with X-rays alone, which became more pronounced at 4 Gy. The most significant effect was achieved with combined treatment at 4 Gy, lowering viability to 53.3%. These findings indicate that BFO-Si NPs potentiate radiation-induced cytotoxicity in lung cancer cells.

Comparable results have been reported with related nanomaterials. For instance, Feng et al. [36] showed that BFO nanocatalysts markedly decreased HeLa cell viability under ultrasound (US) exposure, with prolonged US treatment further amplifying cytotoxicity, underscoring the ability of external stimuli to enhance the therapeutic activity of catalytic nanomaterials. Similarly, Rajaee et al. demonstrated dose-dependent radiosensitization by BFO NPs in MCF-7 cells, where increasing nanoparticle concentrations produced greater reductions in viability under X-ray irradiation **[23].** Collectively, these studies corroborate the radiosensitizing properties of BFO-based nanostructures and support the utility of BFO-Si NPs in enhancing tumor cell sensitivity to radiotherapy.

***Clonogenic assay***

The radiosensitizing efficacy of the synthesized BFO-Si NPs was examined using clonogenic assays. The results showed that the control and BFO-Si NP groups displayed the highest colony numbers, confirming that the NPs alone did not impair cell proliferation and were biocompatible. In contrast, X-ray irradiation alone produced only a modest reduction in colony formation, consistent with its known clinical activity. A pronounced dose-dependent decrease in survival fraction was observed when cells were pretreated with BFO-Si NPs before irradiation (2–8 Gy). At 2 Gy, differences between irradiated cells with or without NPs were minimal; however, at 4 Gy, cells treated with 15 µg/mL BFO-Si NPs displayed significantly lower survival than those exposed to irradiation alone.

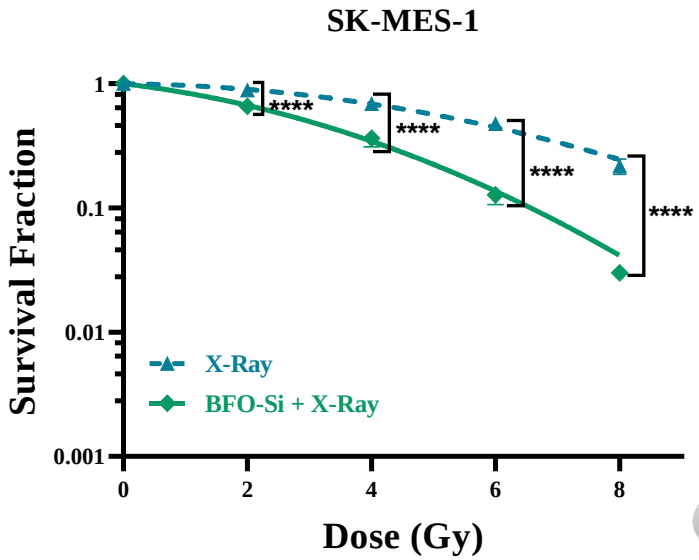


Fig. 5. In vitro clonogenic assay evaluating the effect of BFO-Si NPs on the proliferative capacity of SK-MES-1 cells subjected to varying doses of X-ray irradiation. Values are given as the mean with corresponding standard deviation (n = 3); ****p < 0.0001.

Similar effects were evident at 6 and 8 Gy. For example, pretreatment with 15 µg/mL BFO-Si NPs 6 hours before 6 Gy irradiation reduced the survival fraction (SF6) from 0.47 to 0.12 (Fig. 5). These results demonstrate that BFO-Si NPs substantially enhance X-ray–induced cytotoxicity by suppressing clonogenic survival in a dose-dependent manner. Comparable results have been reported for uncoated BFO NPs. For instance, Rajaee et al. [23] reported that BFO NPs enhanced radiation-induced cytotoxicity in MCF-7 breast cancer cells. A linear-quadratic model predicted sensitizer enhancement ratios (SERs) of 1.35 and 1.76 for 0.05 and 0.1 mg/mL BFO, respectively. At 4 Gy, colony formation decreased from 64% (radiation alone) to 45%, 30%, and 12% with 0.05, 0.1, and 0.2 mg/mL BFO NPs, respectively. These findings highlight the strong radiosensitizing potential of BFO NPs across different cancer cell models. Both studies demonstrate that bismuth ferrite NPs significantly amplify radiation-induced cytotoxicity. However, the BFO-Si system presented here offers additional advantages, as the silica shell is expected to improve nanoparticle stability, dispersibility, and biocompatibility, while also conferring drug delivery potential and imaging capability, thereby providing a more versatile theranostic platform for integrated radiotherapy and drug delivery applications.

***Apoptosis assay with and without X-ray radiation***

Apoptosis induction in SK-MES-1 cells was evaluated using Annexin V-FITC/PI staining followed by flow cytometric analysis. This assessment was performed after cells were subjected to BFO-Si NPs, X-ray irradiation, or their combined application. The results demonstrated that co-treatment with BFO-Si NPs and X-rays markedly increased the percentage of apoptotic cells relative to each modality alone or untreated controls. X-ray irradiation is known to trigger apoptosis, primarily through p53-dependent pathways, and nanoradiosensitizers have been proposed to amplify this response. Accordingly, apoptosis induction in SK-MES-1 cells was quantified following X-ray irradiation at different doses (2 and 4 Gy), with particular emphasis on assessing radiation sensitivity in the presence or absence of the synthesized BFO-Si NPs. As expected, X-ray exposure alone induced apoptosis dose-dependently, rising from 13% to 21.5% as the dose increased from 2 to 4 Gy (Fig. 6B). However, this effect was modest relative to the combined treatment, where apoptosis rose from 26% to 34.3% across the same dose range, indicating that BFO-Si NPs markedly enhanced radiosensitivity.

The radiosensitizing effect of BFO-Si is attributable to the high atomic number of bismuth, which amplifies local energy deposition during irradiation. Secondary photoelectrons and Auger electrons generated upon X-ray interaction with bismuth promote ROS formation, leading to DNA double-strand breaks, oxidative stress, and mitochondrial dysfunction that activate intrinsic apoptotic pathways. The silica shell may further potentiate this response by improving nanoparticle dispersibility and cellular uptake while contributing to ROS generation [20, 21]. These combined effects provide a plausible mechanistic basis for the enhanced apoptosis observed in irradiated cells treated with BFO-Si NPs.

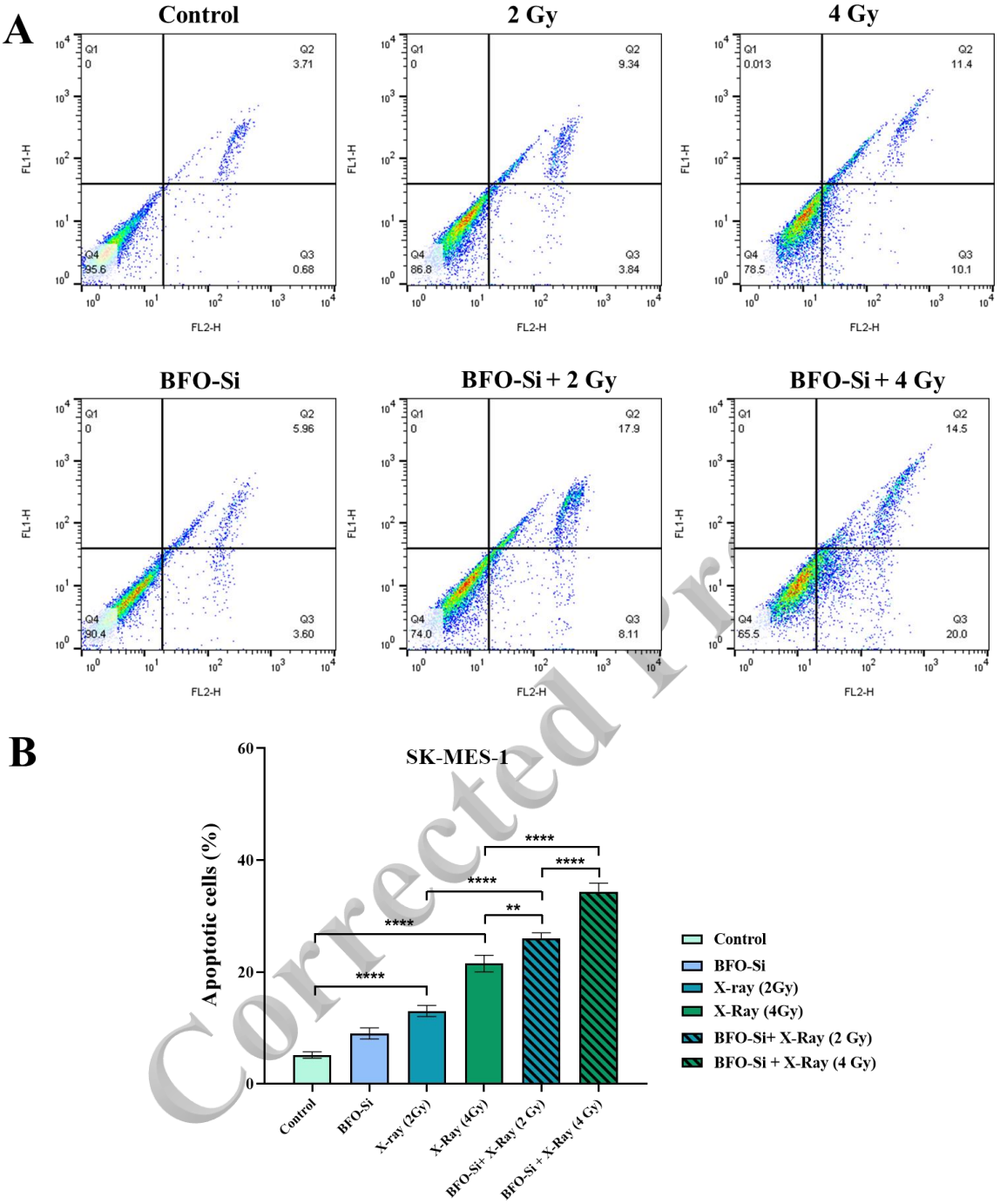


Fig. 6. (A, B) Apoptosis analysis of SK-MES-1 cells exposed to 2 Gy and 4 Gy X-ray irradiation, with or without BFO-Si NPs treatment. Differences were considered statistically significant at ***$p < 0.001$, ****$p < 0.0001$.

Comparable findings have been reported in other studies employing bismuth-based nanomaterials. Specifically, Khosravi et al. [7] observed a significant, dose-dependent enhancement of X-ray-induced apoptosis in colon cancer cells when treated with $Bi_2Se_3$ NPs, primarily through early apoptotic pathways. In contrast, BFO-Si NPs induced early and late apoptosis, suggesting a broader apoptotic impact resulting from ferrite, silica, and bismuth synergistic contributions. Similarly, Faghfoori et al. [37] demonstrated that $Bi_2S_3$@BSA and methotrexate-conjugated $Bi_2S_3$@BSA nanoparticles significantly enhanced apoptosis in SW480 colon cancer cells following irradiation, with the conjugated system showing the most significant effect. Notably, $Bi_2S_3$@BSA NPs exhibited minimal cytotoxicity, but their combination with X-rays pronouncedly increased

apoptotic cell death. These findings highlight the theranostic potential of engineered bismuth nanomaterials and emphasize the importance of synergistic designs in maximizing radiosensitization.

Collectively, these results confirm that bismuth-based nanomaterials can enhance radiation-induced apoptosis in a dose-dependent manner. While $Bi_2Se_3$ and $Bi_2S_3$ systems have demonstrated radiosensitizing efficacy in colon cancer models, the present work provides the first evidence that silica-coated bismuth ferrite (BFO-Si) nanoparticles achieve similar effects in lung cancer cells. Furthermore, the incorporation of ferrite and silica not only contributes to apoptosis induction but also enhances nanoparticle stability, dispersibility, biocompatibility, and potential for drug loading, offering advantages over single-component systems. These results underscore the potential of BFO-Si NPs as multifunctional radiosensitizers for improving the efficacy of lung cancer radiotherapy. Despite these promising findings, a limitation of the present study is that all in vitro experiments were conducted exclusively in SK-MES-1 cells. While these results provide crucial initial evidence of the radiosensitizing potential of BFO–Si NPs, cellular responses to nanomaterials may vary across different tumor types and between malignant and normal cells. Therefore, future studies should validate these findings in additional lung cancer and non-cancerous cell models to establish the broader translational relevance of BFO-Si NP.

## CONCLUSION

This study indicates that the combination of BFO-Si NPs and RT offers a promising therapeutic approach for NSCLC. The low intrinsic cytotoxicity of BFO-Si NPs in cultured cells supports their potential suitability as therapeutic adjuvants. Combined with ionizing radiation, these NPs significantly enhance cellular radiosensitivity, functioning as effective radiosensitizers. Nonetheless, further investigations are needed to elucidate the underlying molecular mechanisms that govern their radiosensitizing effect. Moreover, extensive preclinical evaluations are essential to establish their safety and therapeutic efficacy, with particular attention to potential off-target effects on normal tissues.

## ACKNOWLEDGMENTS

The authors thank the Mashhad University of Medical Sciences for their financial support of this project (Grant No. 4000782).

## AUTHORS CONTRIBUTIONS

Nasim Kavousi: Writing Original Draft, Investigation, Methodology, Data curation, Formal Analysis. Mohammad Taghi Bahreyni Toossi: Funding acquisition, Supervision. Hosein Azimian: Investigation, Methodology. Mona Alibolandi: Project administration, Investigation, Conceptualization, Supervision. All authors read and approved the final manuscript.

## CONFLICTS OF INTEREST

The authors declare no competing interests.

## FUNDING

This study was funded by Grant Number [4000782] from Mashhad University of Medical Sciences, Mashhad, Iran.

## REFERENCES

1. Siegel RL, Miller KD, Jemal A. Cancer statistics, 2019. CA Cancer J Clin. 2019;69(1):7–34.
2. Sung H, Ferlay J, Siegel RL, Laversanne M, Soerjomataram I, Jemal A, et al. Global cancer statistics 2020: GLOBOCAN estimates of incidence and mortality worldwide for 36 cancers in 185 countries. CA Cancer J Clin. 2021;71(3):209–249.
3. Chalela R, Curull V, Enriquez C, Pijuan L, Bellosillo B, Gea J. Lung adenocarcinoma: from molecular basis to genome-guided therapy and immunotherapy. J Thorac Dis. 2017;9(7):2142.
4. Zhao R, Ding D, Yu W, Zhu C, Ding Y. The lung adenocarcinoma microenvironment mining and its prognostic merit. Technol Cancer Res Treat. 2020;19:1533033820977547.
5. De Ruysscher D, Niedermann G, Burnet NG, Siva S, Lee AW, Hegi-Johnson F. Radiotherapy toxicity. Nat Rev Dis Primers. 2019;5(1):13.
6. Moloudi K, Khani A, Najafi M, Azmoonfar R, Azizi M, Nekounam H, et al. Critical parameters to translate gold nanoparticles as radiosensitizing agents into the clinic. Wiley Interdiscip Rev Nanomed Nanobiotechnol. 2023;15(6):e1886.
7. Khosravi H, Manoochehri H, Farmany A, Khoshghadam A, Rafieemehr H, Azmoonfar R. Bismuth selenide nanoparticles enhance radiation sensitivity in colon cancer cells in vitro. Biochem Biophys Rep. 2024;38:101732.
8. Chung YC, Chen IH, Chen CJ. The surface modification of silver nanoparticles by phosphoryl disulfides for improved biocompatibility and intracellular uptake. Biomaterials. 2008;29(12):1807–1816.
9. Verma A, Uzun O, Hu Y, Han HS, Watson N, Chen S, et al. Surface-structure-regulated cell-membrane penetration by monolayer-protected nanoparticles. Nat Mater. 2008;7(7):588–595.
10. Bibb E, Alajlan N, Alsuwailem S, Mitchell B, Brady A, Maqbool M, et al. Internalized nanoceria modify the radiation-sensitivity profile of MDA MB231 breast carcinoma cells. Biology (Basel). 2021;10(11):1148.

11. Shen H, Huang H, Jiang Z. Nanoparticle-based radiosensitization strategies for improving radiation therapy. Front Pharmacol. 2023;14:1145551.
12. Kavousi N, Nazari M, Toossi MTB, Azimian H, Alibolandi M. Smart bismuth-based platform: a focus on radiotherapy and multimodal systems. J Drug Deliv Sci Technol. 2024;101:106136.
13. Shahbazi MA, Faghfouri L, Ferreira MP, Figueiredo P, Maleki H, Sefat F, et al. The versatile biomedical applications of bismuth-based nanoparticles and composites: therapeutic, diagnostic, biosensing, and regenerative properties. Chem Soc Rev. 2020;49(4):1253–321.
14. Catalan G, Scott JF. Physics and applications of bismuth ferrite. Adv Mater. 2009;21(24):2463–85.
15. Wang X, Lin Y, Zhang Z, Bian J. Photocatalytic activities of multiferroic bismuth ferrite nanoparticles prepared by glycol-based sol–gel process. J Sol Gel Sci Technol. 2011;60(1):1–5.
16. Lu AH, Salabas EL, Schüth F. Magnetic nanoparticles: synthesis, protection, functionalization, and application. Angew Chem Int Ed Engl. 2007;46(8):1222–1244.
17. Chandra Sekhar D, Diwakar BS, Madhavi N. Silica coated magnetic nanoparticles for biological applications. Int J Nanosci Nanotechnol. 2020;16(4):209–217.
18. Bagheri E, Naserifar M, Ramezani P, Ramezani M, Alibolandi M. Silica–polymer hybrid nanoparticles for drug delivery and bioimaging. Hybrid Nanomater Drug Deliv. 2022;227–243.
19. Klein S, Dell'Arciprete ML, Wegmann M, Distel LV, Neuhuber W, Gonzalez MC, et al. Oxidized silicon nanoparticles for radiosensitization of cancer and tissue cells. Biochem Biophys Res Commun. 2013;434(2):217–222.
20. Fathy MM, Saad OA, Elshemey WM, Fahmy HM. Dose-enhancement of MCF7 cell line radiotherapy using silica-iron oxide nanocomposite. Biochem Biophys Res Commun. 2022;632:100–106.
21. Chu Y, Wang L, Ke Y, Feng X, Rao W, Ren W, et al. A multifunctional mesoporous silica drug delivery nanosystem that ameliorates tumor hypoxia and increases radiotherapy efficacy. NPG Asia Mater. 2024;16(1):40.
22. Cheng D, Ji Y, Wang B, Wang Y, Tang Y, Fu Y, et al. Dual-responsive nanohybrid based on degradable silica-coated gold nanorods for triple-combination therapy for breast cancer. Acta Biomater. 2021;128:435–446.
23. Rajaee A, Wensheng X, Zhao L, Wang S, Liu Y, Wu Z, et al. Multifunctional bismuth ferrite nanoparticles as magnetic localized dose enhancement in radiotherapy and imaging. J Biomed Nanotechnol. 2018;14(6):1159–11568.
24. Nosrati H, Ghaffarlou M, Salehiabar M, Mousazadeh N, Abhari F, Barsbay M, et al. Magnetite and bismuth sulfide Janus heterostructures as radiosensitizers for in vivo enhanced radiotherapy in breast cancer. Biomater Adv. 2022;140:213090.
25. Xiao J, Zeng L, Ding S, Chen Y, Zhang X, Bian XW, et al. Tumor-tropic adipose-derived mesenchymal stromal cell mediated Bi2Se3 nano-radiosensitizers delivery for targeted radiotherapy of non-small cell lung cancer. Adv Healthc Mater. 2022;11(8):2200143.
26. Catalano E, Miola M, Ferraris S, Novak S, Oltolina F, Cochis A, et al. Magnetite and silica-coated magnetite nanoparticles are highly biocompatible on endothelial cells in vitro. Biomed Phys Eng Express. 2017;3(2):025015.
27. Parvez MM, Haque ME, Akter M, Ferdous H. Synthesis of bismuth ferrite nanoparticles by modified Pechini sol-gel method. Int J Sci Eng Investig. 2020;9(101):35–39.
28. Xiang H, Wu Y, Zhu X, She M, An Q, Zhou R, et al. Highly stable silica-coated bismuth nanoparticles deliver tumor microenvironment-responsive prodrugs to enhance tumor-specific photoradiotherapy. J Am Chem Soc. 2021;143(30):11449–11461.
29. Hasan M, Islam MF, Mahbub R, Hossain MS, Hakim M. A soft chemical route to the synthesis of BiFeO3 nanoparticles with enhanced magnetization. Mater Res Bull. 2016;73:179–186.
30. Zhang CW, Zeng CC, Xu Y. Preparation and characterization of surface-functionalization of silica-coated magnetite nanoparticles for drug delivery. Nano. 2014;9(4):1450042.
31. Verma R, Chauhan A, Batoo KM, Kumar R, Hadhi M, Raslan EH. Effect of calcination temperature on structural and morphological properties of bismuth ferrite nanoparticles. Ceram Int. 2021;47(3):3680–3691.
32. Niloy NR, Chowdhury M, Anowar S, Islam J, Rhaman M. Structural and optical characterization of multiferroic BiFeO3 nanoparticles synthesized at different annealing temperatures. J Mater Sci. 2020;55(12):5000–5012.
33. Fu C, Long X, Cai W, Chen G, Deng X. Structural and magnetic properties of bismuth ferrite nanopowders prepared via sol-gel method. Ferroelectrics. 2014;460(1):157–161.
34. Staedler D, Passemard S, Magouroux T, Rogov A, Maguire CM, Mohamed BM, et al. Cellular uptake and biocompatibility of bismuth ferrite harmonic advanced nanoparticles. Nanomedicine. 2015;11(4):815–824.
35. Song Q, Liu Y, Jiang Z, Tang M, Li N, Wei F, et al. The acute cytotoxicity of bismuth ferrite nanoparticles on PC12 cells. J Nanopart Res. 2014;16(5):2408.
36. Feng L, Gai S, He F, Yang P, Zhao Y. Multifunctional bismuth ferrite nanocatalysts with optical and magnetic functions for ultrasound-enhanced tumor theranostics. ACS Nano. 2020;14(6):7245–7258.
37. Faghfoori MH, Nosrati H, Rezaeejam H, Charmi J, Kaboli S, Johari B, et al. Anticancer effect of X-ray triggered methotrexate conjugated albumin coated bismuth sulfide nanoparticles on SW480 colon cancer cell line. Int J Pharm. 2020;582:119320.